Evaluation of Photochemical Pollution during Transport of Air Pollutants in Spring over the East China Sea

Yasuhiro Sadanaga[1),*], Tadashi Kobashi[1)], Akie Yuba[1),2)], Shungo Kato[3)], Yoshizumi Kajii[4),5)], Akinori Takami[5)] and Hiroshi Bandow[1)]

[1)]Department of Applied Chemistry, Graduate School of Engineering, Osaka Prefecture University, 1-1 Gakuen-cho, Naka-ku, Sakai, Osaka 599-8531, Japan
[2)]Now at Asia Center for Air Pollution Research, 1182 Sowa, Nishi-ku, Niigata, Niigata 950-2144, Japan
[3)]Division of Applied Chemistry, Faculty of Urban Environmental Sciences, Tokyo Metropolitan University, 1-1 Minami-Ohsawa, Hachioji, Tokyo 192-0397, Japan
[4)]Graduate School of Global Environmental Studies, Kyoto University, Yoshida-nihonmatsu-cho, Sakyo-ku, Kyoto, Kyoto 606-8501, Japan
[5)]National Institute for Environmental Studies, 16-2 Onogawa, Tsukuba, Ibaraki 305-8506, Japan

*Corresponding author. Tel: +81-72-254-9326, E-mail: sadanaga@chem.osakafu-u.ac.jp

ABSTRACT

We conducted intensive observations of ozone, CO, NO_x (=NO and NO_2), NO_y (total odd nitrogen species including particulate nitrate) and total nitrate (the sum of gaseous HNO_3 and particulate nitrate) at Cape Hedo, Okinawa, Japan, from 19 March to 3 April, 2009, to investigate ozone production during long-range transport from the Asian continent. Ozone production efficiency (OPE) was used to evaluate photochemical ozone production. OPE is defined as the number of molecules of ozone produced photochemically during the lifetime of a NO_x molecule. OPE is calculated by the ratio of the concentration increase of ozone to that of NO_z (= $NO_y - NO_x$). Average OPE during observation was estimated to be 12.6 ± 0.5, but concentrations of ozone increased nonlinearly with those of NO_z. This non-linearity suggests that OPE depends on air mass origin and NO_z concentrations. There were very different values of OPE for the same air mass origin, so that only the air mass origin alone does not control OPE. OPE was low when NO_z concentration was high. We examined the correlation between NO_z and CO/NO_y ratios, which we used instead of the ratio of non-methane hydrocarbons (NMHCs) to NO_x. The CO/NO_y ratios decreased with increasing NO_z concentrations. These results indicate that competition reactions of OH with NMHCs and NO_2 are the rate determining steps of photochemical ozone production during long-range transport from the Asian continent to Cape Hedo, for high concentrations of nitrogen oxides.

Key words: Ozone production efficiency, Total odd nitrogen species, Long-range transport, East Asia, Non-methane hydrocarbons

1. INTRODUCTION

Recent remarkable economic progress in East Asia has caused an increase in NO_x (=NO + NO_2) emissions (e.g. Akimoto, 2003). Ohara *et al.* (2007) developed an emission inventory for Asia (Regional Emission Inventory in Asia: REAS), and reported that Asian NO_x emissions increased by 176% from 1980 to 2003. In particular, NO_x emissions in China showed a marked increase of 280%. More recently, Kurokawa *et al.* (2013) updated REAS emission inventory (REAS ver. 2) and estimated that NO_x emissions in Asia and China increased by 54 and 89%, respectively, from 2000 to 2008. Zhang *et al.* (2007) estimated a NO_x emission increase by 70% in China from 1995 to 2004. Satellite observations show that NO_2 column densities increased by 95% from 1996 to 2004 (Zhang *et al.*, 2007).

Atmospheric pollutants such as NO_x emitted in East Asia are transported with chemical transformations and can affect the environmental quality of other regions directly and indirectly (e.g. Takiguchi *et al.*, 2008). A representative effect is photochemical pollution such as ozone. Suthawaree *et al.* (2008) performed continuous observations of ozone and CO at Cape Hedo, Okinawa, Japan. They described long-range transport of ozone and CO from the Asian continent using backward trajectory analyses, and suggested photochemical production of ozone during the transport because of a positive correlation between ozone and CO. Episodic pollution of photochemical ozone was observed over Japan in spring (8-9 May 2007). Ohara *et al.* (2008) concluded that this episode was strongly influenced by trans-boundary air pollutants such as nitrogen oxides and volatile organic compounds emitted on the Asian

continent. Long-term monitoring of springtime ozone at a site on Mount Happo, Japan, has shown increase at a rate of ~1 ppbv (part per billion by volume) y^{-1}. One reason for this increase is considered to be an indirect effect caused by rapidly increasing anthropogenic emissions of NO_x from East Asia (Tanimoto, 2009).
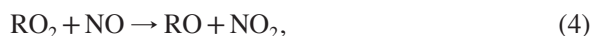
Photochemical ozone production is nonlinear against the precursors of ozone such as NO_x and non-methane hydrocarbons (NMHCs). Ozone in the troposphere is generated in the photolysis of NO_2:
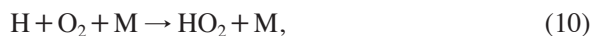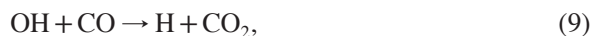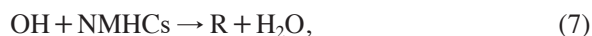
$$NO_2 + h\nu \, (\lambda < 420 \, nm) \rightarrow NO + O \, (^3P), \tag{1}$$

$$O \, (^3P) + O_2 + M \rightarrow O_3 + M, \tag{2}$$

where M represents third-body molecules such as N_2 and O_2. The inverse of reactions (1) and (2) regenerates NO_2 and destroys ozone:

$$NO + O_3 \rightarrow NO_2 + O_2. \tag{3}$$

Photochemical ozone production is substantially controlled by the reaction of NO with peroxy radicals (RO_2; R means an organic group):

$$RO_2 + NO \rightarrow RO + NO_2, \tag{4}$$

$$RO + O_2 \rightarrow HO_2 + carbonyl \, compounds, \tag{5}$$

$$HO_2 + NO \rightarrow OH + NO_2. \tag{6}$$

Reactions (1)-(6) form the photostationary state of NO_x during daytime. Peroxy radicals are generated by the reaction of OH with NMHCs and CO:

$$OH + NMHCs \rightarrow R + H_2O, \tag{7}$$

$$R + O_2 + M \rightarrow RO_2 + M, \tag{8}$$

$$OH + CO \rightarrow H + CO_2, \tag{9}$$

$$H + O_2 + M \rightarrow HO_2 + M, \tag{10}$$

Reactions (4)-(10) form a chain reaction centered on $RO_x \, (= OH + HO_2 + RO_2)$ radicals to generate tropospheric ozone. NMHCs act as a propagator of the chain reaction. On the other hand, NO_x acts as a terminator as well as propagator of the chain reaction while NO_x is the direct precursor of ozone. NO_2 reacts with OH to generate nitric acid:

$$OH + NO_2 + M \rightarrow HNO_3 + M. \tag{11}$$
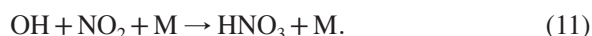
In the case of low NO_x mixing ratios, the rate-determining steps of the photochemical ozone production are reactions (4) and (6), so that ozone production rates rise when NO_x concentrations increase. In the case of high NO_x mixing ratios, the rate-determining steps are shifted to the peroxy radical regeneration (reactions (7) and (9)). Reactions (7) and (9) have a competing reaction (11), which acts as a terminator of the chain reac-
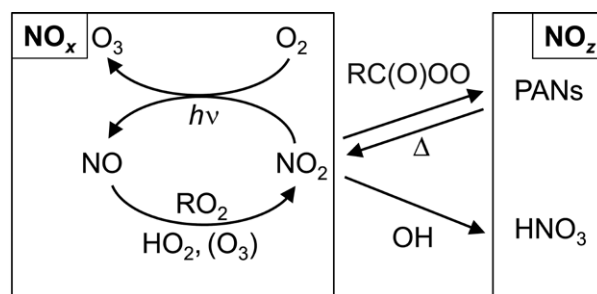
Fig. 1. Mechanism of ozone production chain reactions in view of nitrogen oxides.

tion. The increase of NO_x concentrations makes favorable for reaction (11), so that ozone production rates decrease. An important factor of photochemical ozone production is the NMHCs/NO_x ratio, because the ozone production rate is determined with respect to the branching ratio between reactions (7) and (11).

To clarify behavior of ozone for long-range transport, it is necessary to discuss the ozone production rate as well as the ozone concentration level. Ozone production efficiency (OPE) is an important parameter for addressing ozone production rate (e.g. Ge *et al*., 2013; Chou *et al*., 2009; Kleinman *et al*., 1994). OPE is defined as the "number of ozone molecules per NO_x molecule oxidized". Fig. 1 shows ozone production chain reactions in view of nitrogen oxides. Nitrogen oxides are emitted as NO_x and ozone is photochemically produced by the NO_x-RO_x chain reaction in Fig. 1. Ozone is produced as long as the chain reaction proceeds. On the other hand, NO_2 reacts with OH and peroxyacyl radicals (RC(O)OO) to produce HNO_3 and PANs, respectively. Total odd nitrogen species (NO_y) other than NO_x such as HNO_3 and PANs are called NO_z (i.e. $NO_z = NO_y - NO_x$), which is more stable than NO_x and does not contribute directly to ozone production. The reactions of NO_z production are equivalent to the termination reaction of photochemical ozone production. In summary, a NO_x molecule produces several ozone molecules via oxidation from NO_x to NO_z and the number of ozone molecules is defined as OPE. Thus, OPE is expressed as the ratio of concentration increment of ozone ($\Delta[O_3]$) to that of NO_z ($\Delta[NO_z]$):

$$OPE = \frac{\Delta[O_3]}{\Delta[NO_z]}. \tag{12}$$

To diagnose ozone production during long-range transport from the Asian continent, we performed intensive observation of NO_2 using a laser-induced fluorescence technique at the National Institute for Environmental Studies Cape Hedo Atmosphere and Aerosol Monitoring Station (CHAAMS), Okinawa, Japan. Ozone, CO, NO,

NO_y and total nitrate (TN = the sum of gaseous HNO_3 and particulate nitrate) are observed continuously at CHAAMS. We investigated OPE during the transport using data observed, and discussed the contributing factor when determining the value of OPE.

2. EXPERIMENTAL

2. 1 Site Description

The CHAAMS observation site is at latitude 26° 52′N, longitude 128°15′E, and an elevation 60 m above sea level (Fig. 2). Details of the site are described elsewhere (Suthawaree *et al.*, 2008; Takiguchi *et al.*, 2008; Takami *et al.*, 2007; Kanaya *et al.*, 2001). Briefly, it is located near Cape Hedo, the northernmost point of the Okinawa main island and is about 100 km from Naha City, which is the largest city on that island. The site is about 20 km from the center of Kunigami Village, population ~6000. Horizontal distance from the site to the seashore is only about 200 m to the northwest. The site is in the remote marine boundary layer and is suitable to diagnose air pollution by long-range transport from East Asia. Observation was carried out from 19 March to 3 April 2009.

2. 2 Measurement Species

Ozone, CO and NO were measured using commercially available instruments based on UV absorption (Model 49i; Thermo Fisher Scientific), a non-dispersive infrared photometer (Model 48C; Thermo Electron) and NO-ozone chemiluminescence (Model 42i-TL; Thermo Fisher Scientific), respectively. For the CO measurement, zero air generated from a heated Pt catalyst (Model 96, Nippon Thermo) was measured during the first 20 min of every hour, to check the zero point of the CO analyzer (Suthawaree *et al.*, 2008). NO_y was observed by a molybdenum catalyst followed by NO-ozone chemiluminescent detection (Sadanaga *et al.*, 2008a; Williams *et al.*, 1998). The fraction of particulate nitrate in NO_y reaches 50% at CHAAMS. A large part of particulate nitrate around CHAAMS is in coarse mode (Takiguchi *et al.*, 2008), which would mainly originate from uptake of gaseous HNO_3 on the surface of sea salt. The NO_y measured at CHAAMS includes a large portion of particulate nitrate because a molybdenum catalyst reduces $NaNO_3$ quantitatively to NO (Sadanaga *et al.*, 2008b). The detection limits of ozone, NO, CO and NO_y are 1 (according to the operation manual), 0.045 (3σ), 17 (3σ) and 0.045 (3σ) ppbv, respectively.

TN was measured by the scrubber difference/NO-ozone chemiluminescence method (Yuba *et al.*, 2010; Sadanaga *et al.*, 2008a; Tanner *et al.*, 1998). Briefly,
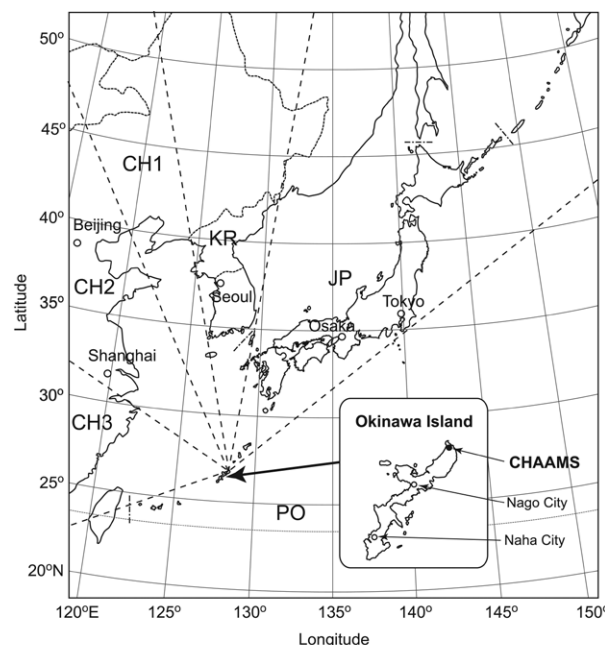
Fig. 2. Map of East Asia and CHAAMS location. Dashed lines indicate classification of air mass origin (see Section 2.3).

ambient air was passed through a Teflon filter to remove particles and then introduced to an annular denuder coated with NaCl to remove gaseous HNO_3 before entering the other molybdenum catalyst followed by the NO-ozone chemiluminescent detector. The $NO_y - TN$ concentration was measured by this method. The TN concentration can be obtained by subtracting the $NO_y - TN$ concentration from the NO_y concentration:

$$[TN] = [NO_y] - [NO_y - TN]. \qquad (13)$$

The detection limit of TN is the same as that of HNO_3 analyzer reported previously (Sadanaga *et al.*, 2008a). The detection limit depends on NO_y concentration and was estimated to be 71 pptv with 10-min integration time (2σ) under NO_y concentration of 5 ppbv (Sadanaga *et al.*, 2008a).

NO_2 was measured using a laser-induced fluorescence technique (LIF). The detailed principle and instrumentation of the LIF are described elsewhere (Sadanaga *et al.*, 2004; Matsumoto and Kajii, 2003). Briefly, ambient air was introduced to the fluorescence detection cell through an orifice of diameter 0.254 mm. In this cell, a second harmonic of the solid-state pulsed Nd:YAG laser (Awave-532 nm-8W-10 kHz; Advanced Optowave) was irradiated to excite NO_2 molecules. The YAG laser has a repetition rate of 10 kHz, pulse width 76 ns, beam diameter 1 mm and maximum output 7 W during observation. Fluctuation of laser power

was monitored outside the detection cell using a photodiode (S1226-5BQ; Hamamatsu) to correct the sensitivity of this LIF system fluctuated by the laser power. The cell was pumped by a rotary pump (RV8; Edwards) to reduce quenching of excited NO_2. Pressure in the cell was approximately 330 Pa, measured using a capacitance manometer (Model 720; Setra).

Fluorescence emitted from the excitation volume is focused onto a photocathode of a dynode-gated photomultiplier tube (R928P; Hamamatsu) through two lenses and a sharp-cutoff filter (R62; Asahi Technoglass), which was used to cut off scattered light to the photomultiplier tube. In addition, the photomultiplier tube was time-gated to distinguish between scattered light and fluorescence using a normally off dynode gating system (C1392-56; Hamamatsu). The gating system was controlled by a positive transistor-transistor logic (TTL) pulse, which is generated by a delay/pulse generator (DG535; Stanford Research Systems). The negative output signal from the photomultiplier tube is led to an amplification/discrimination unit (C9744; Hamamatsu) to convert to positive TTL pulses. The number of these pulses in a single gate period is counted by a photon counting board (M8784; Hamamatsu), that is slotted in a master computer (Dimension 8250; Dell). Typical gate timing for photon counting is between 0.3 and 3.1 µs after the laser pulse. The detection limit of the NO_2-LIF instrument during intensive observation is 53 pptv (parts per trillion by volume) at $S/N = 2$, with an integration time of 60 s and laser power 7 W.

NMHCs were analyzed by a Gas Chromatograph-Flame Ionization Detector (GC-FID) (HP 6890; Hewlett Packard) (Kato *et al*., 2004, 2001). Ambient air samples were collected into 6 L stainless canisters for NMHCs analyses. The sampled air of 500 cm^3 was concentrated into a three-stage pre-concentrator (Entech7000; Entech) prior to the injection into the GC-FID. GC column was HP-1 (60-m length, 0.32-mm inner diameter and 1-µm film thickness). Initially GC oven temperature was kept at $-50°C$ (for 8 min) and then increased to $40°C$ at the rate of $5°C\,min^{-1}$, after that further increased to $150°C$ at $15°C\,min^{-1}$. NMHC concentrations were calibrated with 1 ppmv standard gas containing 58 species (PAMS-J58; Sumitomoseika). Detection limits of the NMHCs are in the range of 1-3 pptv with 2-13% accuracy and 2-15% precision.

2. 3 Backward Trajectory Analysis

Backward trajectory analyses were performed using the HYSPLIT 4 model developed by the American National Oceanic and Atmospheric Administration (NOAA) (Draxler and Rolph, 2012; Rolph, 2012). Initial altitude and calculation time were set at 500 m and 120 hours, respectively. Origins of air masses reaching the observational site were classified into six groups, based on the last coastline passed. The origins are described in Fig. 2: North China (CH1), Middle China (CH2), South China (CH3), Korea (KR), Japan (JP) and the Pacific Ocean (PO). Air masses that meandered or did not belong to any of above origins were excluded from analysis. Trajectory data were gathered every six hours: 3:00, 9:00, 15:00 and 21:00 Japan Standard Time (JST). The NO_y and HNO_3 concentrations were averaged into 6-hour bins to classify them into air masses identified by backward trajectory. Concentration data of 0:00-6:00, 6:00-12:00, 12:00-18:00 and 18:00-24:00 correspond to trajectories of 3:00, 9:00, 15:00 and 21:00, respectively.

3. RESULTS AND DISCUSSION

3. 1 Overview

Fig. 3 shows observed data of ozone, NO_y, TN, NO, NO_2 and CO from 19 March to 3 April 2009. Average concentrations of ozone, NO_y, TN, NO, NO_2 and CO were 50.0, 1.02, 0.44, 0.02, 0.20 and 180.8 ppbv, respectively. Large peak concentrations of ozone, NO_y, TN and CO were observed around 21:00 on 22 March. Backward trajectory analysis indicates that the air mass in this period came from the Asian continent via the Shanghai area. Unfortunately, NO_2 concentrations between 21 and 23 March were missing data because of problems with the laser system. The second-highest peak concentrations of ozone, NO_y, TN and CO during the observation were observed between 1 and 3 April. The backward trajectory analyses indicate that the air masses in these periods originated between CH2 and KR. Concentration variations of NO_y were similar to those of TN as shown in Fig. 3(a). The air mass around CHAAMS was well-aged, and these concentration peaks are due to the outflow of Asian pollutants.
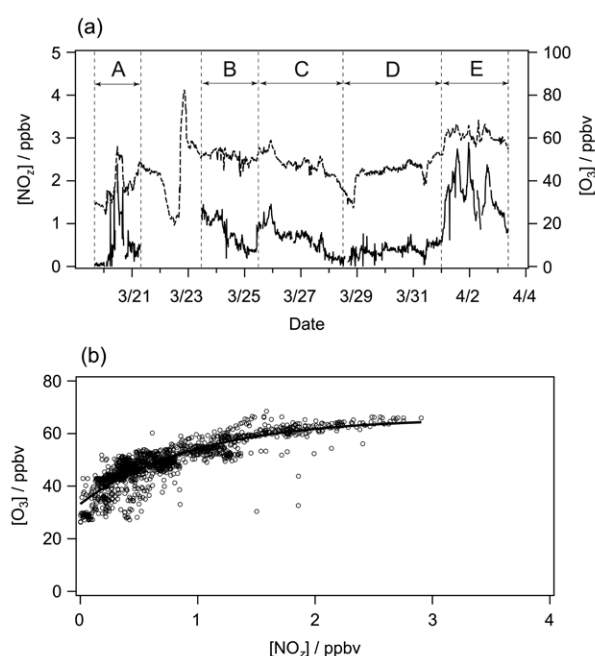
3. 2 Estimation of OPE

Fig. 4(a) shows daily variations of NO_z and ozone concentrations. The highest concentration period of NO_z was from 1 to 3 April and ozone concentration during this period was also highest, save for a large peak concentration on 22 March. Fig. 4(b) shows that the ozone concentration was positively correlated with the NO_z concentration. The slope of the regression line is defined to be OPE. In this case, OPE during the observation period was estimated at 12.6 ± 0.5. However, ozone concentrations increased nonlinearly with NO_z concentrations. This result suggests that OPE is dependent on air masses and NO_z concentrations. Analyses of OPE using air mass classification and NO_y concen-
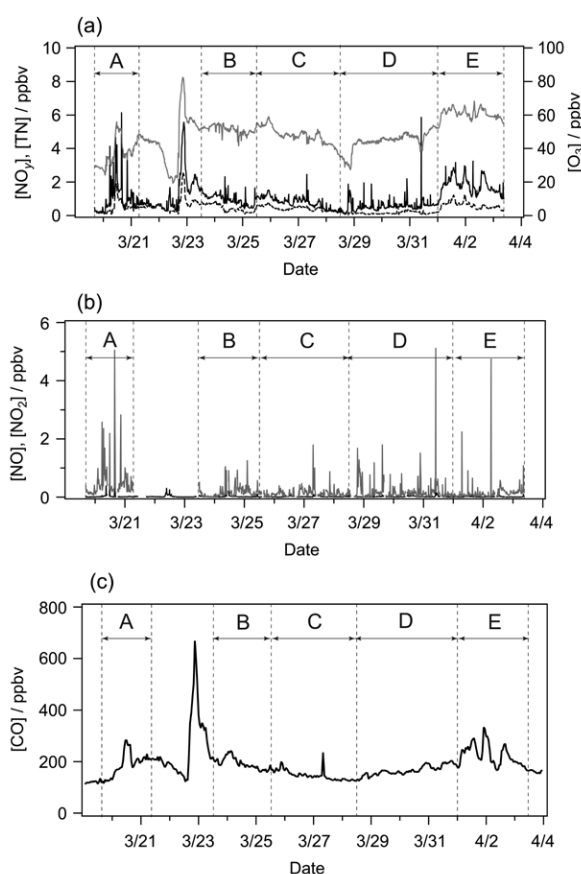
Fig. 3. (a) Daily variations of ozone (gray line), NO_y (solid line) and TN (dashed line) concentrations. Each plot represents 10-min average values. (b) Daily variations of NO (solid line) and NO_2 (gray line) concentrations. Each plot represents 10-min average values. (c) Daily variation of CO concentration. Each plot represents 1-h average values. A to E mean periods A to E (see section 3.3).

**Fig. 4.** (a) Daily variations of ozone (dashed line) and NO_z (solid line) concentrations. Each plot represents 10-min average values. A to E mean periods A to E (see section 3.3). (b) Relationship between ozone and NO_z concentrations. Solid curve shows just guide to eye.

trations are described in Section 3.3.

In previous studies, OPE was reported to be about 10 in areas of low NO_x concentrations (Kleinman *et al.*, 1994; Olszyna *et al.*, 1994). On the other hand, OPEs in the urban areas of New York, Nashville and Beijing were estimated from 2-4 (Kleinman *et al.*, 2000), 3-6 (St. John *et al.*, 1998) and 1.0-6.8 (Ge *et al.*, 2013), respectively, which are lower than those in the clean atmosphere. At the remote area in East Asia, for example, averaged OPE was estimated to be 10 at Oki Island, Japan (Jaffe *et al.*, 1996). NO_x concentrations at CHAAMS are low, and the OPE of 12.6 around the site is consistent with the earlier reports. OPE estimated by this method is inferred under the assumption that deposition velocities of ozone and NO_z are the same. In reality, the NO_z deposition velocity is larger than that of ozone in most cases (Section 3.4). It should be

noted that OPE estimated by this method shows the upper limit (Nunnermacker *et al.*, 1998).

3.3 Variation of OPE with Air Masses

As described in the preceding section, correlation between ozone and NO_z was nonlinear. The plot of Fig. 4(b) seems to be composed by several linear relationships between ozone and NO_z. This intensive observation can be divided into the following five periods by air mass origins obtained by backward trajectory analyses: 19 through 21 March (period A, PO air mass origin), 23 through 25 March (period B, KR-JP air mass origin), 25 through 28 March (period C, CH1-CH2 air mass origin), 28 through 31 March (period D, JP air mass origin) and 1 through 3 April (period E, CH1-CH2 air mass origin). Fig. 5 shows relationships between ozone and NO_z within each category. Linear correlations were obtained for each period. OPEs ranged widely, from 4.7 to 24.2. As seen in Fig. 5(c) and (e), OPEs were very different between periods C (OPE = 14.56) and E (OPE = 4.83), despite the fact that air masses in both periods had from the same origin, CH1-CH2. Therefore, OPE is not determined by air mass origin only.
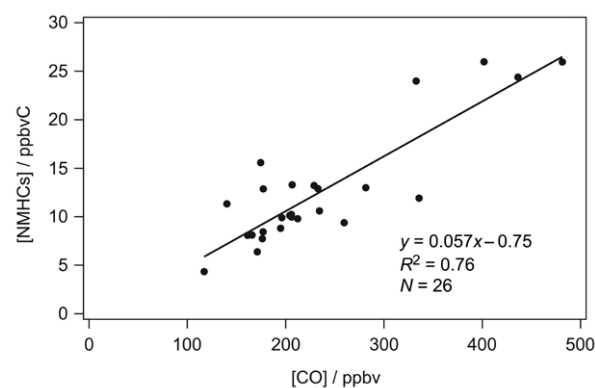
It is noteworthy that OPE decreases when the NO_z concentration is high. For example, OPE for period A
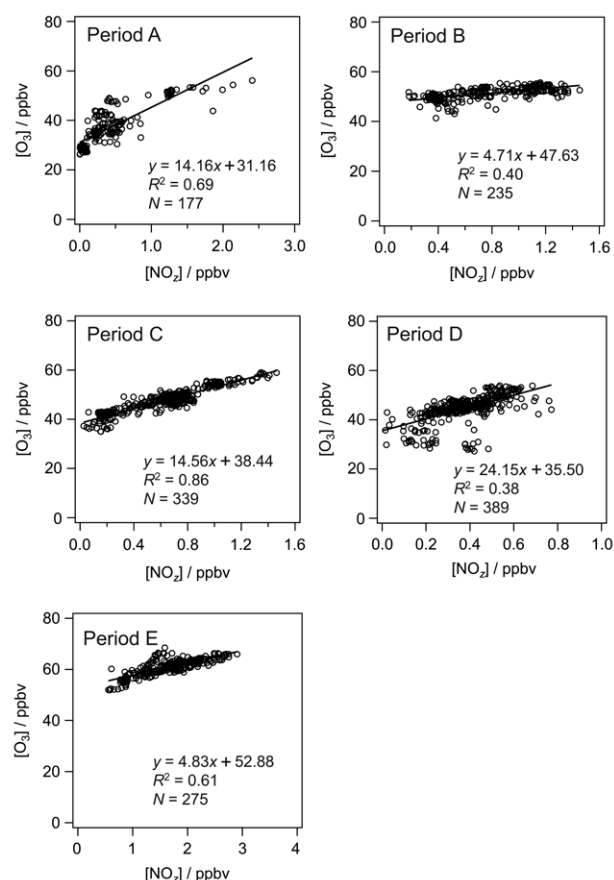
Fig. 5. Relationships between ozone and NO_z concentrations from 19 to 21 March (period A, PO air mass origin), 23 to 25 March (period B, KR-JP air mass origin), 25 to 28 March (period C, CH1-CH2 air mass origin), 28 to 31 March (period D, JP air mass origin) and 1 to 3 April (period E, CH1-CH2 air mass origin). Solid lines represent regression lines. N means the number of data.


Fig. 6. Correlation between CO and NMHC concentrations measured at CHAAMS. ppbvC means parts per billion by volume carbon basis. Solid line is the regression line. N means the number of data.

Table 1. Summary of measured NMHCs at Cape Hedo in spring 2006.

Chemicals	Species
Alkane	ethane, propane, *n*-butane, *i*-butane, *n*-pentane, *i*-pentane, *n*-hexane, heptane, octane, nonane
Alkene	ethylene, propylene, 1-butene, cis-2-butene, trans-2-butene, 1-3-butadiene, 3-methyl-1-butene
Alkyne	acetylene
Aromatics	benzene, toluene, ethylbenzene, *o*-xylene, *m-p*-xylene
Biogenic	isoprene, α-pinene, β-pinene, limonene, camphene

was estimated at 14.16. However, OPE decreased to 2.03 in the same period when using only data of NO_z concentrations more than 1 ppbv. As described above, OPE for period E was much lower than that for period C. The NO_z concentration for period E was much greater than that for period C, while the air masses originated from CH1-CH2 in both periods. In the previous studies, OPEs in polluted air were lower than those in the clean atmosphere (Section 3.2).

To investigate the relationship between OPE and the NO_z concentration, we examined correlation between NO_z and NMHCs/NO_x ratios (Sadanaga *et al*., 2012). As described in Section 1, an important factor of photochemical ozone production is the NMHCs/NO_x ratio, which indicates that ozone production rate is determined with respect to the branching ratio between reactions (7) and (11). Unfortunately, NMHC concentrations were not continuously observed during the study period, so we used CO concentrations instead. CO concentrations have good correlation with those of NMHCs originating from combustion processes. Indeed, there was good correlation between CO and NMHCs measured at CHAAMS from 16 to 20 March and from 4 to 13 April 2006 (Fig. 6). Table 1 shows NMHCs measured in spring 2006. NO_y concentrations were used instead of NO_x to analyze the relationship between NO_z concentrations and NMHCs/NO_x ratios. The lifetime of NO_x is so short that most NO_x emitted from the Asian continent is oxidized to NO_y during transport to CHAAMS. To discuss photochemical ozone production during the transport process, the use of NO_y instead of NO_x is more appropriate.

CO/NO_y ratios decreased with increasing NO_z concentrations (Fig. 7(a)). Considering the mechanisms of photochemical ozone production, decreases in both
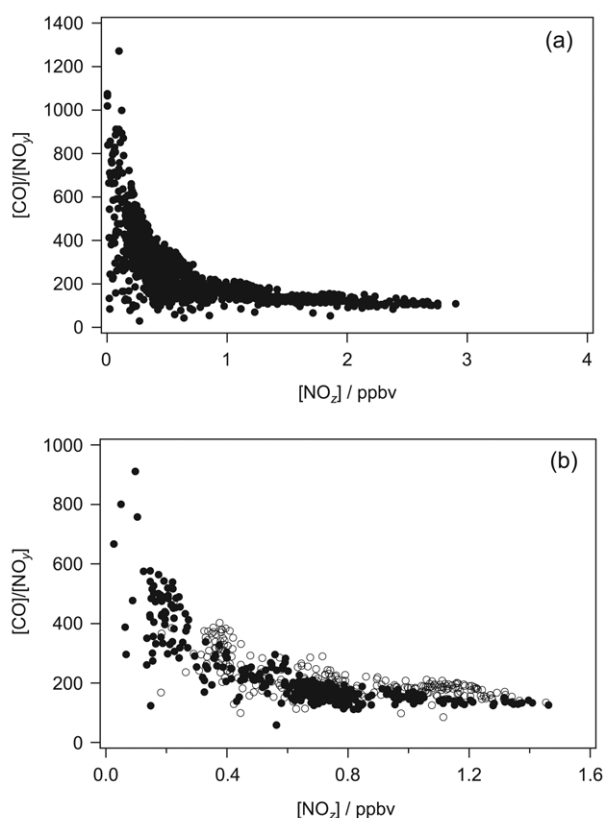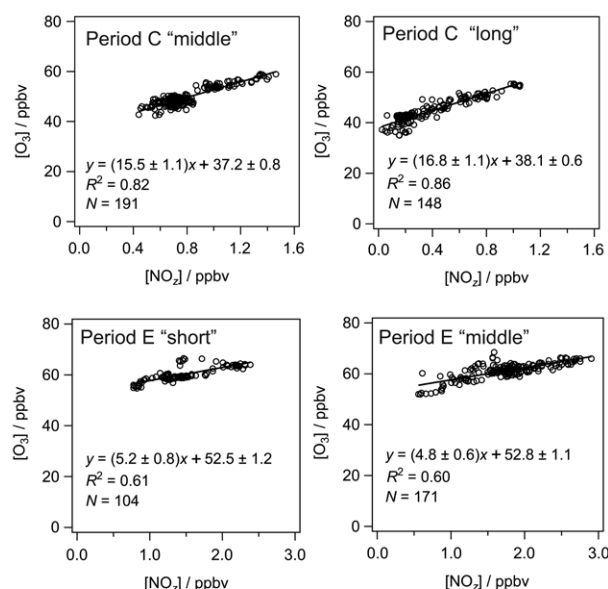
Fig. 7. Relationship between the CO/NO$_y$ ratios and NO$_z$ concentrations for (a) entire observation period, and (b) periods B (open circles) and C (filled circles).

Fig. 8. Correlation between NO$_z$ and ozone concentrations measured at CHAAMS in periods C and E, categorized by transport time: short (0-29 hours), middle (30-59 hours), and long (60 hours or more) groups. Solid lines represent regression lines. Errors show two standard deviations (2σ). N means the number of data.

CO/NO$_y$ ratio and OPE with increasing NO$_z$ suggest that competition reactions of OH with NMHCs and NO$_2$ (i.e., reactions (7) and (11)) are the rate determining steps for photochemical ozone production during the transport to CHAAMS, at least for high concentrations of nitrogen oxides. We also investigated the relationships between NO$_z$ concentrations and CO/NO$_y$ ratios for periods B and C, which have similar NO$_z$ concentrations but different OPEs. The CO/NO$_y$ ratios for period B were higher than those for period C (Fig. 7(b)), whereas OPE for period B was lower than that for period C (Fig. 5(b) and (c)). Reasons for this result may be differences of air mass origin, NMHC composition, meteorological conditions and others, but we cannot draw clear conclusions at this time. It is expected that the accumulation of NMHC as well as NO$_z$ and ozone data will clarify OPEs during transport over East Asia.

3. 4 Influence of Transport Time on OPE

As described in Section 3.2, OPE estimates were inferred under the assumption that deposition veloci-

ties of ozone and NO$_z$ are the same. Thus, these deposition velocities might influence OPE values. The deposition velocity of NO$_z$ depends on its constituents. The main components in NO$_z$ observed around CHAAMS were reported to be gaseous nitric acid and coarse particulate nitrate (Takiguchi *et al*., 2008), whose deposition velocities are greater than that of ozone (Lovett, 1994). Indeed, about half of NO$_y$ was total nitrate in this observation. These results indicate that the deposition velocity of NO$_z$ is greater than that of ozone. Therefore, the OPE values estimated by this method show the upper limit as described in Section 3.2 and may be overestimated. The difference of deposition velocities influences the apparent OPEs more strongly in the case of longer transport time from the Asian continent to CHAAMS. From this view-point, the relationship between OPEs and transport time was investigated. The transport time was defined as the air mass travel duration from the last Asian continental coastline to CHAAMS. This is also the time spent over the sea, and can be calculated from the backward trajectory analysis. We categorized the transport time into "short" (0-29 hours), "middle" (30-59 hours), and "long" (60 hours or more) groups.

OPEs can be affected by air mass origins and NO$_z$ concentration as well as transport time, so the relationship between OPEs and transport time should be

investigated over the same periods. Fig. 8 shows correlations between OPEs and transport time in periods C (Fig. 8(a)) and E (Fig. 8(b)), when both air masses originated from CH1-CH2. In period C, transport times were long and fell into only the middle and long groups. OPE in the middle group was in agreement with that in the long group within statistical errors. In period E, transport times were short and fell into only the short and middle groups. An OPE difference was not observed with statistical significance between the short and the middle groups. Given these results, we concluded that OPE is more strongly affected by NO_z concentration and air mass origin than by NO_z deposition during long-range transport.

4. CONCLUSIONS

Intensive observations of ozone, CO, NO_x, NO_y and TN were carried out at CHAAMS, Okinawa, Japan, from 19 March to 3 April 2009. Average concentrations of ozone, NO_y, TN, NO, NO_2 and CO were 50.0, 1.02, 0.44 0.02, 0.20 and 180.8 ppbv, respectively. The concentration of NO_z was positively correlated with that of ozone. OPE was estimated from the regression line slope. Average OPE was estimated at 12.6 ± 0.5 during the observation period, and it was confirmed that ozone concentration increased nonlinearly with that of NO_z. Both OPE and NO_x concentrations obtained demonstrate that CHAAMS is in a remote area.

We investigated OPEs for various air masses arriving at CHAAMS, via classification according to air mass origin and period using backward trajectory analyses. OPEs were very different between the periods 25-28 March (OPE = 14.56) and 1-3 April (OPE = 4.83), despite the same air mass origin (CH1-CH2). Therefore, air mass origin is not the sole determinant of OPE. OPE tends to be small when NO_z concentration is high, regardless of air mass origin. This suggests that NO_z concentration influences OPE. We investigated the relationship between NO_z and ratios of CO/NO_y, which were used instead of $NMHCs/NO_x$ ratios. The CO/NO_y ratios decreased with increasing NO_z concentrations, so the competition reactions of OH with NMHCs and NO_2 could be the rate determining steps for photochemical ozone production during transport from the Asian continent to CHAAMS, at least for high concentrations of nitrogen oxides.

The OPE obtained herein may be overestimated, because the deposition velocity of NO_y is generally greater than that of ozone. The component in NO_y that has the largest deposition velocity is TN, so the apparent value of OPE may increase with transport time from the Asian continent to CHAAMS. We categorized transport time into short (0-29 hours), middle (30-59 hours), and long (60 hours or more) groups, and compared the group OPEs with the same period and air mass origin. There were no significant differences of OPEs between groups. We concluded that OPE is most affected by NO_z concentration and that the influence of the NO_z deposition velocity during transport was not great during the observation period.

ACKNOWLEDGEMENT

REFERENCES

Akimoto, H. (2003) Global air quality and pollution. Science 302, 1716-1719.

Chou, C.C.-K., Tsai, C.-Y., Shiu C.-J., Liu, S.C., Zhu, T. (2009) Measurement of NO_y during Campaign of Air Quality Research in Beijing 2006 (CAREBeijing-2006): Implications for the ozone production efficiency of NO_x. Journal of Geophysical Research 114, D00G01, doi:/10.1029/ 2008JD010446.

Draxler, R.R., Rolph, G.D. (2012) HYSPLIT (Hybrid Single-Particles Lagrangian Integrated Trajectory) Model access via NOAA ARL READY Website (http://ready.arl.noaa.gov/HYSPLIT.php). NOAA Air Resources Laboratory, Silver Spring, MD.

Ge, B., Sun, Y., Liu, Y., Dong, H., Ji, D., Jiang, Q., Li, J., Wang, Z. (2013) Nitrogen dioxide measurement by cavity attenuated phase shift spectroscopy (CAPS) and implications in ozone production efficiency and nitrate formation in Beijing, China. Journal of Geophysical Research Atmospheres 118, 9499-9509.

Jaffe, D.A., Honrath, R.E., Zhang, L., Akimoto, H., Shimizu, A., Mukai, H., Murano, K., Hatakeyama, S., Merrill, J. (1996) Measurements of NO, NO_y, CO and O_3 and estimation of the ozone production rate at Oki Island, Japan, during PEM-West, Journal of Geophysical Research 101, 2037-2048.

Kanaya, Y., Sadanaga, Y., Nakamura, K., Akimoto, H. (2001) Behavior of OH and HO_2 radicals during the

Observation at a Remote Island of Okinawa (ORION99) field campaign 1. Observation using a laser-induced fluorescence instrument. Journal of Geophysical Research 106, 24197-24208.

Kato, S., Pochanart, P., Kajii, Y. (2001) Measurements of ozone and non-methane hydrocarbons at Chichi-jima island, a remote island in the western Pacific: Long-range transport of polluted air from the Pacific rim region. Atmospheric Environment 35, 6021-6029.

Kato, S., Kajii, Y., Itokazu, R., Hirokawa, J., Koda, S., Kinjo, Y. (2004) Transport of atmospheric carbon monoxide, ozone, and hydrocarbons from Chinese coast to Okinawa island in the Western Pacific during winter. Atmospheric Environment 38, 2975-2981.

Kleinman, L.I., Lee, Y.-N., Springston, S.R., Nunnermacker, L., Zhou, X., Brown, R., Hallock, K., Klotz, P., Leahy, D., Lee, J.H., Newman, L. (1994) Ozone formation at a rural site in the southeastern United States. Journal of Geophysical Research 99, 3469-3482.

Kleinman, L.I., Daum, P.H., Imre, D.G., Lee, J.H., Lee, Y.-N., Nunnermacker, L.J., Springston, S.R., Weinstein-Lloyd, J., Newman, L. (2000) Ozone production in the New York City Urban Plume. Journal of Geophysical Research 105, 14495-14511.

Kurokawa, J., Ohara, T., Morikawa, T., Hatayama, S., Janssens-Maenhout, G., Fukui, T., Kawashima, K., Akimoto, H. (2013) Emissions of air pollutants and greenhouse gases over Asian regions during 2000-2008: Regional Emission inventory in ASia (REAS) version 2. Atmospheric Chemistry and Physics 13, 11019-11058.

Lovett, G.M. (1994) Atmospheric deposition of nutrients and pollutants in North America. Ecological Applications 4, 629-650.

Matsumoto, J., Kajii, Y. (2003) Improved analyzer for nitrogen dioxide by laser-induced fluorescence technique. Atmospheric Environment 37, 4847-4851.

Nunnermacker, L.J., Imre, D., Daum, P.H., Kleinman, L., Lee, Y.-N., Lee, J.H., Springston, S.R., Newman, L., Weinstein-Lloyd, J., Luke, W.T., Banta, R., Alvarez, R., Senff, C., Sillman, S., Holdren, M., Keigley, G.W., Zhou, X. (1998) Characterization of the Nashville urban plume on July 3 and July 18, 1995. Journal of Geophysical Research 103, 28129-28148.

Ohara, T., Akimoto, H., Kurokawa, J., Horii, N., Yamaji, K., Yan, X., Hayasaka, T. (2007) An Asian emission inventory of anthropogenic emission sources for the period 1980-2020. Atmospheric Chemistry and Physics 7, 4419-4444.

Ohara, T., Uno, I., Kurokawa, J., Hayasaki, M., Shimizu, A. (2008) Episodic pollution of photochemical ozone during 8-9 May 2007 over Japan - Overview -. Journal of Japan Society for Atmospheric Environment 43, 198-208 (in Japanese).

Olszyna, K.J., Bailey, E.M., Simonaitis, R., Meagher J.F. (1994) O_3 and NO_y relationships at a rural site. Journal of Geophysical Research 99, 14557-14563.

Rolph, G.D. (2012) Real-time Environmental Applications Display sYstem (READY) Website (http://ready.arl.noaa.gov). NOAA Air Resources Laboratory, Silver Spring, MD.

Sadanaga, Y., Matsumoto, J., Sakurai, K., Isozaki, R., Kato, S., Nomaguchi, T., Bandow, H., Kajii, Y. (2004) Development of a measurement system of peroxy radicals using a chemical amplification/laser-induced fluorescence technique. Review of Scientific Instruments 75, 864-872.

Sadanaga, Y., Yuba, A., Kawakami, J., Takenaka, N., Yamamoto, M., Bandow, H. (2008a) A gaseous nitric acid analyzer for the remote atmosphere based on the scrubber difference/NO-ozone chemiluminescence method. Analytical Sciences 24, 967-971.

Sadanaga, Y., Imabayashi, H., Suzue, T., Kimoto, H., Kimoto, T., Takenaka, N., Bandow, H. (2008b) Quantitative reduction of particulate nitrate to nitric oxide by a molybdenum catalyst: Implications for NO_y measurements in the marine boundary layer. Geophysical Research Letters 35, L21810, doi:10.1029/2008GL035557.

Sadanaga, Y., Sengen, M., Takenaka, N., Bandow, H. (2012) Analyses of the ozone weekend effect in Tokyo, Japan: Regime of oxidant ($O_3 + NO_2$) production. Aerosol Air Quality Research 12, 161-168.

St. John, J.C., Chameides, W.L., Saylor, R. (1998) Role of anthropogenic NO_x and VOC as ozone precursors: A case study from the SOS Nashville/Middle Tennessee Ozone Study. Journal of Geophysical Research 103, 22415-22423.

Suthawaree, J., Kato, S., Takami, A., Kadena, H., Toguchi, M., Yogi, K., Hatakeyama, S., Kajii, Y. (2008). Observation of ozone and carbon monoxide at Cape Hedo, Japan: Seasonal variation and influence of long-range transport. Atmospheric Environment 42, 2971-2981.

Takami, A., Miyoshi, T., Shimono, A., Kaneyasu, N., Kato, S., Kajii, Y., Hatakeyama, S. (2007) Transport of anthoropogenic aerosols from Asia and subsequent chemical transformation. Journal of Geophysical Research 112, D22S31, doi:10.1029/2006JD008120.

Takiguchi, Y., Takami, A., Sadanaga, Y., Lun, X., Shimizu, A., Matsui, I., Sugimoto, N., Wang, W., Bandow, H., Hatakeyama, S. (2008) Transport and transformation of total reactive nitrogen over the East China Sea. Journal of Geophysical Research 113, D10306, doi:10.1029/2007JD09462.

Tanimoto, H. (2009) Increase in springtime tropospheric ozone at a mountainous site in Japan for the period 1998-2006. Atmospheric Environment 43, 1358-1363.

Tanner, R.L., Valente, R.J., Meagher, J.F. (1998) Measuring inorganic nitrate species with short time resolution an aircraft platform by dual-channel ozone chemiluminescence. Journal of Geophysical Research 103, 22387-22395.

Williams, E.J., Baumann, K., Roberts, J.M., Bertman, S.B., Norton, R.B., Fehsenfeld, F.C., Springston, S.R., Nunnermacker, L.J., Newman, L., Olszyna, K., Meag-

her, J., Hartsell, B., Edgerton, E., Pearson, J.R., Rodgers, M.O. (1998) Intercomparison of ground-based NO_y measurement techniques. Journal of Geophysical Research 103, 22261-22280.

Yuba, A., Sadanaga, Y., Takami, A., Hatakeyama, S., Takenaka, N., Bandow, H. (2010) Measurement system for particulate nitrate based on the scrubber difference NO-O_3 chemiluminescence method in remote areas. Analytical Chemistry 82, 8916-8921.

Zhang, Q., Streets, D.G., He, K., Wang, Y., Richter, A., Burrows, J.P., Uno, I., Jang, C.J., Chen, D., Yao, Z., Lei, Y. (2007) NO_x emission trends for China, 1995-2004: The view from the ground and the view from space. Journal of Geophysical Research 112, D22306, doi:10.1029/ 2007JD008684.